

Numerical Study of Approximation Techniques for the Temporal Weights to the DWR Method

Marius Paul Bruchhäuser* · Markus Bause†

Helmut Schmidt University, University of the German Federal Armed Forces Hamburg,
Faculty of Mechanical and Civil Engineering, Chair of Numerical Mathematics
Holstenhofweg 85, 22043 Hamburg, Germany

Abstract

This work presents a numerical investigation of different approximation techniques for the temporal weights used in the Dual Weighted Residual (DWR) method applied to a time-dependent convection-diffusion equation which is assumed to be convection-dominated. It is a continuation of a previous work by the authors where spatial weights were compared for a steady-state case. A higher-order finite elements approach is compared to a more cost-efficient higher-order reconstruction approach. Numerical examples point out the results regarding accuracy, efficiency and stability reasons.

Keywords: Goal-Oriented A Posteriori Error Control · Dual Weighted Residual Method · Temporal Weights · Convection-Dominated Problems · SUPG Stabilization

1 Introduction

The DWR method has attracted researchers' interest in many fields of application problems since it was introduced by Becker and Rannacher [1, 2] at the turn of the last millennium, cf., e.g., [3, 4, 5]. In order to obtain efficient, adaptive meshes in space and time, the DWR approach yields an a posteriori error estimator measured in goal quantities of physical interest. To get such an error estimator, an additional *dual* problem has to be solved, which is used for *weighting* the influence of local *residuals* on the error. In this respect, the approximation of these weights is crucial. As shown in a comparative numerical study by the authors in [6], in particular considering convection-dominated problems, the differences between different approximation techniques for the spatial weights can be significant regarding accuracy and efficiency reasons. In this work, the focus is now on the numerical investigation of different approximation approaches for the temporal weights. Thus, we consider the following time-dependent convection-diffusion-reaction equation given by

$$\begin{aligned} \partial_t u - \nabla \cdot (\varepsilon \nabla u) + \mathbf{b} \cdot \nabla u + \alpha u &= f \quad \text{in } Q = \Omega \times I, \\ u(0) &= u_0 \quad \text{on } \Sigma_0 = \Omega \times \{0\}, \end{aligned} \tag{1.1}$$

equipped with appropriate boundary conditions. We denote by Q the space-time domain, where $\Omega \subset \mathbb{R}^d$, with $d = 2$ or $d = 3$, is a polygonal or polyhedral bounded domain with Lipschitz boundary $\partial\Omega$ and $I = (0, T)$, $0 < T < \infty$, is a finite time interval. Well-posedness

*bruchhaeuser@hsu-hamburg.de (*corresponding author)

†bause@hsu-hamburg.de

of (1.1) and the existence of a sufficiently regular solution, such that all of the arguments and terms used below are well-defined, are tacitly assumed without mentioning explicitly all technical assumptions about the data and coefficients here; cf., e.g., [7] and [8, Ch. 4] for the details. Henceforth, for the sake of simplicity, we deal with homogeneous Dirichlet boundary values, $u|_{\partial\Omega} = 0$. In our numerical examples, we also consider more general boundary conditions, whose incorporation is straightforward, cf. [8, Rem. 4.14].

This work is organized as follows. In Sec. 2, we present the weak form as well as the (stabilized) space-time discretization schemes. In Sec. 3, we derive an a posteriori error representation for the model problem. In Sec. 4, we introduce two different approximation techniques for the temporal weights and present the underlying space-time adaptive algorithm. Finally, in Sec. 5, the results of our numerical comparison study are presented.

2 Variational Formulation and Discretization in Space and Time

Introducing the function space $V := \{v \in L^2(I; H_0^1(\Omega)) \mid \partial_t v \in L^2(I; H^{-1}(\Omega))\}$, the variational formulation of problem (1.1) reads as follows: *Find $u \in V$ such that*

$$A(u)(\varphi) := \int_I \{(\partial_t u, \varphi) + a(u)(\varphi)\} dt + (u(0) - u_0, \varphi(0)) = \int_I (f, \varphi) dt =: F(\varphi) \quad (2.1)$$

for all $\varphi \in V$, with an inner bilinear form $a(u)(\varphi) := (\varepsilon \nabla u, \nabla \varphi) + (\mathbf{b} \cdot \nabla u, \varphi) + (\alpha u, \varphi)$. For the discretization in time we use a discontinuous Galerkin method dG(r) with an arbitrary polynomial degree $r \geq 0$. Let $0 =: t_0 < t_1 < \dots < t_N =: T$ be a set of time points for a partition of I into left-open subintervals $I_n := (t_{n-1}, t_n]$, $n = 1, \dots, N$, with time step sizes $\tau_n = t_n - t_{n-1}$ and global discretization parameter $\tau = \max_n \tau_n$. Thus, the space-time domain Q is separated into a partition of tensor-product slabs $Q = \Omega \times I_n$. Let $V_\tau^r := \{u_\tau \in L^2(I; H_0^1(\Omega)) \mid u_\tau|_{I_n} \in \mathcal{P}_r(I_n; H_0^1(\Omega)), u_\tau(0) \in L^2(\Omega)\}$, where $\mathcal{P}_r(I_n; H_0^1(\Omega))$ is the space of polynomials up to degree r on I_n with values in $H_0^1(\Omega)$. Then, the semi-discrete in time scheme reads as follows: *Find $u_\tau \in V_\tau^r$ such that*

$$A_\tau(u_\tau)(\varphi_\tau) + (u_{\tau,0}^+ - u_0, \varphi_{\tau,0}^+) = F(\varphi_\tau) \quad \forall \varphi_\tau \in V_\tau^r, \quad (2.2)$$

with $F(\cdot)$ being defined in (2.1) and the semi-discrete bilinear form $A_\tau(\cdot)(\cdot)$ given by

$$A_\tau(u_\tau)(\varphi_\tau) := \sum_{n=1}^N \int_{I_n} \{(\partial_t u_\tau, \varphi_\tau) + a(u_\tau)(\varphi_\tau)\} dt + \sum_{n=2}^N ([u_\tau]_{n-1}, \varphi_{\tau,n-1}^+). \quad (2.3)$$

Here, the jump $[\cdot]_n$ at a time point t_n for some discontinuous in time function $u_\tau \in V_\tau^r$ is defined by $[u_\tau]_n := u_{\tau,n}^+ - u_{\tau,n}^-$, with $u_{\tau,n}^\pm := \lim_{t \rightarrow t_n \pm 0} u_\tau(t)$.

For the discretization in space, we use a standard continuous Galerkin method cG(p) with an arbitrary polynomial degree $p \geq 1$. For this, we consider a decomposition \mathcal{T}_h of the domain Ω into disjoint elements K , such that $\bar{\Omega} = \cup_{K \in \mathcal{T}_h} \bar{K}$. Here, we choose the elements $K \in \mathcal{T}_h$ to be quadrilaterals ($d = 2$) or hexahedrals ($d = 3$). We denote by h_K the diameter of K and the global space discretization parameter is $h := \max_{K \in \mathcal{T}_h} h_K$. Our mesh adaptation process yields locally refined cells, which is enabled by using hanging nodes; cf. [9] for further details. Let $V_{\tau h}^{r,p} := \{u_{\tau h} \in V_\tau^r \mid u_{\tau h}|_{I_n} \in \mathcal{P}_r(I_n; V_h^{p,n}), u_{\tau h}(0) \in V_h^{p,0}\}$ be the fully discrete function space. Now, the fully discrete scheme is given by replacing the semi-discrete functions in (2.2) by the fully discrete ones. In the implementation we are using tensor-product polynomials on a single slab, cf. [14] for the details. Since we focus on convection-dominated problems here, the finite element approximation needs to be stabilized in order to reduce spurious and non-physical oscillations arising close to layers. Here, we use the streamline upwind

Petrov-Galerkin (SUPG) method [10, 11]. Finally, the stabilized fully discrete scheme reads as follows: Find $u_{\tau h} \in V_{\tau h}^{r,p}$ such that

$$A_S(u_{\tau h})(\varphi_{\tau h}) + (u_{\tau h,0}^+ - u_0, \varphi_{\tau h,0}^+) = F(\varphi_{\tau h}) \quad \forall \varphi_{\tau h} \in V_{\tau h}^{r,p}, \quad (2.4)$$

where $A_S(u_{\tau h})(\varphi_{\tau h}) := A_\tau(u_{\tau h})(\varphi_{\tau h}) + S_A(u_{\tau h})(\varphi_{\tau h})$, with $A_\tau(\cdot)(\cdot)$ being defined in (2.3) and $S_A(\cdot)(\cdot)$ are the SUPG stabilization terms being defined in the Appendix.

3 DWR-Based A Posteriori Error Estimation

In this section, we present a DWR-based a posteriori error representation for the stabilized problem (2.4). This representation is given in terms of a user chosen goal functional, in general given as $J(u) = \int_0^T J_1(u(t)) dt + J_2(u(T))$, where $J_1 \in L^2(I; H^{-1}(\Omega))$ and $J_2 \in H^{-1}(\Omega)$ are three times differentiable functionals and each of them may be zero; cf., e.g., [12]. In order to keep this work short, we restrict this section to the main result only and refer to [8, Ch. 4.2] for a detailed derivation.

Theorem 3.1 (Temporal and Spatial Error Representation)

Let $\{u, z\} \in V \times V$, $\{u_\tau, z_\tau\} \in V_\tau^r \times V_\tau^r$, and $\{u_{\tau h}, z_{\tau h}\} \in V_{\tau h}^{r,p} \times V_{\tau h}^{r,p}$ be stationary points of Lagrangian functionals \mathcal{L} , \mathcal{L}_τ , and $\mathcal{L}_{\tau h}$ on different discretization levels

$$\begin{aligned} \mathcal{L}'(u, z)(\delta u, \delta z) = \mathcal{L}'_\tau(u, z)(\delta u, \delta z) = 0 & \quad \forall \{\delta u, \delta z\} \in V \times V, \\ \mathcal{L}'_\tau(u_\tau, z_\tau)(\delta u_\tau, \delta z_\tau) = 0 & \quad \forall \{\delta u_\tau, \delta z_\tau\} \in V_\tau^r \times V_\tau^r, \\ \mathcal{L}'_{\tau h}(u_{\tau h}, z_{\tau h})(\delta u_{\tau h}, \delta z_{\tau h}) = 0 & \quad \forall \{\delta u_{\tau h}, \delta z_{\tau h}\} \in V_{\tau h}^{r,p} \times V_{\tau h}^{r,p}. \end{aligned}$$

Then, there holds the error representation formulas in space and time, respectively,

$$\begin{aligned} J(u) - J(u_\tau) &= \rho_\tau(u_\tau)(z - \tilde{z}_\tau) + \frac{1}{2}\Delta\rho_\tau + \mathcal{R}_\tau, \\ J(u_\tau) - J(u_{\tau h}) &= \rho_\tau(u_{\tau h})(z_\tau - \tilde{z}_{\tau h}) + S_A(u_{\tau h})(\tilde{z}_{\tau h}) + \frac{1}{2}\Delta\rho_h + \mathcal{R}_h, \end{aligned} \quad (3.1)$$

where ρ_τ denotes the primal residual based on the semi-discrete schemes (2.2). Here, $\tilde{z}_\tau \in V_\tau^r$ and $\tilde{z}_{\tau h} \in V_{\tau h}^{r,p}$ can be chosen arbitrarily and $\mathcal{R}_\tau, \mathcal{R}_h$ are higher-order remainder terms with respect to the errors $u - u_\tau, z - z_\tau$ and $u_\tau - u_{\tau h}, z_\tau - z_{\tau h}$. The explicit presentations of \mathcal{L} , \mathcal{L}_τ , $\mathcal{L}_{\tau h}$ and ρ_τ are given in the Appendix.

Proof. The proof includes a result regarding the relation between the primal and dual residual that goes back to [2, Prop. 2.3]. A detailed derivation of this relation for the convection-diffusion equation can be found in [8, Ch. 4.2.2]. \blacksquare

4 Practical Aspects

The error representation formulas derived in the previous section lead to a posteriori error estimators in space and time, whereby the latter serve as indicators for the adaptive mesh refinement process. Therefore, we present a localized form of the reduced error representation formulas. Neglecting the higher-order remainder terms in Thm. 3.1, we get the following error representation formulas in space and time.

$$\begin{aligned} J(u) - J(u_\tau) &\approx \rho_\tau(u_\tau)(z - \tilde{z}_\tau) & =: \eta_\tau = \sum_{n=1}^N \eta_\tau^n, \\ J(u_\tau) - J(u_{\tau h}) &\approx \rho_\tau(u_{\tau h})(z_\tau - \tilde{z}_{\tau h}) + S_A(u_{\tau h})(\tilde{z}_{\tau h}) & =: \eta_h = \sum_{n=1}^N \eta_h^n, \end{aligned} \quad (4.1)$$

where η_τ^n and η_h^n denote the local error indicators with regard to a single slab $Q_n = \mathcal{T}_{h,n} \times I_n, n = 1, \dots, N$; cf. [8, Ch. 4.3.2] for a detailed representation. These indicators include unknown solutions as well as temporal and spatial weights given by $z - \tilde{z}_\tau$ and $z_\tau - \tilde{z}_{\tau h}$, respectively, that have to be approximated by an appropriate technique; cf., e.g., [9, 13, 8]. Due to the results of a comprehensive numerical comparison study with regard to steady-state convection-dominated problems in [6, 8], we use a higher-order finite elements approach for approximating the spatial weights in our numerical examples. Now, in this work, we put the focus on the approximation of the temporal weights by comparing different approximation techniques similar to the steady-state case. In the following, we will shortly introduce these different approximation techniques, where we refer to [8, Ch. 4.3.2] for more details.

Approximation by Higher-Order Reconstruction (for short, hoRe approach)

For the higher-order reconstruction approach, we introduce the following operator

$$z - \tilde{z}_\tau \approx E_\tau^{r+1} z_\tau - z_\tau,$$

where E_τ^{r+1} denotes a reconstruction in time operator that acts on I_n and lifts the solution to a piecewise polynomial of degree $(r + 1)$ in time, cf. Fig. 4.1.

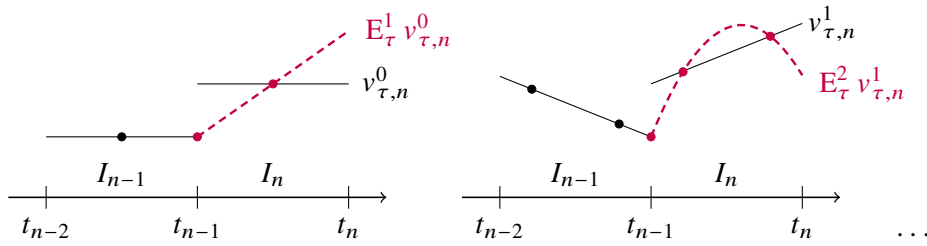


Figure 4.1: Reconstruction of a discontinuous constant (left) and linear (right) in time function using Gauss quadrature points.

Approximation by Higher-Order Finite Elements (for short, hoFE approach)

This approach aims to increase the influence of the weights by approximating the dual solution using higher-order finite elements, i.e. z_τ is computed in $V_\tau^s, s \geq r+1$. Therefore, we introduce the following restriction operator in time given by

$$z - \tilde{z}_\tau \approx z_\tau - R_\tau^r z_\tau,$$

where R_τ^r acts on I_n and restricts the solution to a polynomial of degree $r < s$; cf. Fig. 4.2. Note that this approximation is valid, since the quantity \tilde{z}_τ can be chosen arbitrarily in the finite element space V_τ^s .

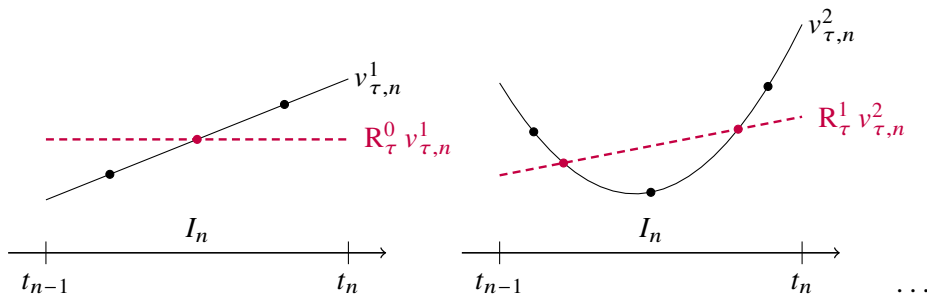


Figure 4.2: Restriction of a discontinuous linear (left) and quadratic (right) in time function using Gauss quadrature points.

Now, the last step in making the error indicators computable is to replace all unknown solutions in Eqs. (4.1) by the computed fully discrete solutions, i.e. we approximate

$$\begin{aligned}\eta_\tau &\approx \rho_\tau(u_{\tau h})(E_\tau^{r+1} z_{\tau h} - z_{\tau h}) =: \tilde{\eta}_\tau^{\text{hoRe}}, \text{ or} \\ \eta_\tau &\approx \rho_\tau(u_{\tau h})(z_{\tau h} - \mathbf{R}_\tau^r z_{\tau h}) =: \tilde{\eta}_\tau^{\text{hoFE}}, \text{ and} \\ \eta_h &\approx \rho_\tau(u_{\tau h})(z_{\tau h} - \mathbf{R}_h^p z_{\tau h}) + S_A(u_{\tau h})(\mathbf{R}_h^p z_{\tau h}) =: \tilde{\eta}_h,\end{aligned}\tag{4.2}$$

where \mathbf{R}_h^p denotes a restriction in space operator that acts on a spatial cell and restricts the solution to a polynomial of degree $p < q$ on the corresponding reference element; cf., e.g., [9, 8]. Finally, we present a survey-like version of our adaptive solution algorithm using tensor-product space-time slabs Q_n , where we refer to [8, Ch. 4.3.3] and [14] for a more detailed version and further information.

Algorithm: Goal-Oriented Space-Time Adaptivity

1. Set $\ell = 1$ and generate initial space-time slabs $Q_n^1 = \mathcal{T}_{h,n}^1 \times I_n^1, n = 1, \dots, N^1$.
2. Compute $u_{\tau h}^\ell$ by solving the **stabilized primal** problem (2.4).
3. Compute $z_{\tau h}^\ell$ by solving the **stabilized dual** problem (6.2).
4. Evaluate the a posteriori space-time **error indicators** η_τ^ℓ and η_h^ℓ .
 - if** $|\eta_\tau^\ell| > \omega |\eta_h^\ell|, 1.5 \leq \omega \leq 3.5$: Adapt the **temporal** mesh only.
 - else if** $|\eta_h^\ell| > \omega |\eta_\tau^\ell|$: Adapt the **spatial** mesh only.
 - else**: Adapt both the **temporal** as well as the **spatial** mesh.
5. Increase ℓ to $\ell + 1$ and return to step 2.

5 Numerical Examples

In this section, we investigate our space-time adaptive algorithm with regard to the different approximation techniques of the temporal weights introduced in the previous section. Thereby, we study accuracy, efficiency as well as stability properties by means of two numerical examples. The first one is an academic test problem including some challenging behavior in time, whereas the second one deals with a benchmark problem of convection-dominated transport problems. In order to focus on the results, we restrict the description of the test settings to a minimum and refer to [8] for the details. For measuring the accuracy of the error estimator, we consider an effectivity index $\mathcal{I}_{\text{eff}} := \left| \frac{\tilde{\eta}_\tau + \tilde{\eta}_h}{J(u) - J(u_{\tau h})} \right|$. Moreover, in the second example the SUPG stabilization parameter is given by $\delta_K = \delta_0 \cdot h_K$, $0.1 \leq \delta_0 \leq 1$, where h_K denotes the cell diameter of the spatial mesh cell K , cf. Rem. 6.1.

Example 1: Rotating Hill with Changing Orientation As first example, we consider a counterclockwise rotating hill on the unit square $\Omega = (0, 1)^2$, which additionally changes its height and orientation over the period $T = 1$. The corresponding exact solution is given by (cf. [8, Ex. 4.2])

$$u(\mathbf{x}, t) := \frac{1 + a \cdot ((x_1 - m_1(t))^2 + (x_2 - m_2(t))^2)}{v_1(t) \cdot s \cdot \arctan(v_2(t))}\tag{5.1}$$

with $m_1(t) := \frac{1}{2} + \frac{1}{4} \cos(2\pi t)$ and $m_2(t) := \frac{1}{2} + \frac{1}{4} \sin(2\pi t)$, and, $v_1(\hat{t}) := -1, v_2(\hat{t}) := 5\pi \cdot (4\hat{t} - 1)$, for $\hat{t} \in [0, 0.5)$ and $v_1(\hat{t}) := 1, v_2(\hat{t}) := 5\pi \cdot (4(\hat{t} - 0.5) - 1)$, for $\hat{t} \in [0.5, 1)$, $\hat{t} = t - k, k \in \mathbf{N}_0$, and, scalars $s = \frac{1}{3}, a_0 = 50$. We choose $\varepsilon = 1, \mathbf{b} = (2, 3)^\top$ and

$\alpha = 1$. Furthermore, no stabilization ($\delta_K = 0$) is used in this test case. The goal quantity is chosen to control the global $L^2(L^2)$ -error in space and time of $e := u - u_{\tau h}$, given by $J_Q(u) = \frac{1}{\|e\|_{(0,T)\times\Omega}} \int_I (u, e) dt$. In Tables 5.1–5.2, we present the results obtained by the two different approximation techniques. Here, N denotes the total number of slabs, N_K^{\max} the number of cells on the finest spatial mesh within the current loop, and $N_{\text{DoF}}^{\text{tot}}$ the total space-time degrees of freedom. Further, $e^{p,r,q,s}$ or rather a $cG(p)$ - $dG(r)$ / $cG(q)$ - $dG(s)$ discretization corresponds to a primal solution approximation $u_{\tau h}^{p,r}$ in $cG(p)$ - $dG(r)$ and a dual solution approximation $z_{\tau h}^{q,s}$ in $cG(q)$ - $dG(s)$.

Regarding the accuracy of the underlying error estimator, as given by the last column of Tables 5.1–5.2, it can be summarized that both approaches show a good quantitative estimation of the discretization error as the respective effectivity index \mathcal{I}_{eff} is around one for all underlying discretization cases. We note slightly better results using the hoRE approach regarding accuracy and stability of the underlying estimators. With regard to efficiency reasons it is essential to ensure an equilibrated reduction of the temporal as well as spatial discretization error. Referring to this, we point out a good equilibration of the spatial and temporal error indicators $\tilde{\eta}_h$ and $\tilde{\eta}_\tau$ in the course of the refinement process (columns six and seven of Tables 5.1–5.2).

ℓ	cG(1)-dG(0)/cG(2)-dG(0)							cG(2)-dG(1)/cG(3)-dG(1)						
	N	N_K^{\max}	$N_{\text{DoF}}^{\text{tot}}$	$J(e^{1,0,2,0})$	$\tilde{\eta}_h$	$\tilde{\eta}_\tau^{\text{hoRe}}$	\mathcal{I}_{eff}	N	N_K^{\max}	$N_{\text{DoF}}^{\text{tot}}$	$J(e^{1,1,2,1})$	$\tilde{\eta}_h$	$\tilde{\eta}_\tau^{\text{hoRe}}$	\mathcal{I}_{eff}
1	25	16	625	2.74e-02	1.89e-02	5.11e-03	0.88	20	16	1000	2.49e-02	2.55e-02	5.54e-04	1.04
2	25	40	1067	1.57e-02	6.72e-03	4.58e-03	0.72	20	40	1724	1.19e-02	1.08e-02	1.15e-03	1.01
3	31	100	3039	8.74e-03	3.08e-03	7.36e-03	1.19	20	88	3404	7.83e-03	6.81e-03	1.55e-03	1.06
4	37	100	3583	7.18e-03	3.73e-03	8.19e-03	1.65	20	148	5352	5.64e-03	3.34e-03	2.01e-03	0.95
5	44	100	4210	6.92e-03	3.87e-03	5.62e-03	1.37	20	256	7600	4.83e-03	1.66e-03	2.54e-03	0.87
6	52	160	7408	4.66e-03	1.85e-03	3.73e-03	1.19	37	256	14266	2.57e-03	2.40e-03	3.98e-04	1.08
7	62	160	8864	4.56e-03	1.87e-03	2.76e-03	1.01	37	424	19190	2.09e-03	1.70e-03	4.96e-04	1.04
8	88	208	15276	3.24e-03	1.19e-03	2.20e-03	1.04	37	724	29182	1.84e-03	1.01e-03	5.53e-04	0.85

Table 5.1: Adaptive refinement including effectivity indices with goal quantity J_Q , $\varepsilon = 1$, $\delta_0 = 0$, and $\omega = 1.5$ for Example 1, using a **higher-order reconstruction** strategy for the temporal weights.

ℓ	cG(1)-dG(0)/cG(2)-dG(1)							cG(1)-dG(1)/cG(2)-dG(2)						
	N	N_K^{\max}	$N_{\text{DoF}}^{\text{tot}}$	$J(e^{1,0,2,1})$	$\tilde{\eta}_h$	$\tilde{\eta}_\tau^{\text{hoRe}}$	\mathcal{I}_{eff}	N	N_K^{\max}	$N_{\text{DoF}}^{\text{tot}}$	$j(e^{1,1,2,2})$	$\tilde{\eta}_h$	$\tilde{\eta}_\tau^{\text{hoRe}}$	\mathcal{I}_{eff}
1	25	16	625	2.74e-02	2.18e-02	1.10e-02	1.19	20	16	1000	2.49e-02	2.63e-02	1.27e-03	1.10
2	25	40	1053	1.58e-02	8.98e-03	1.89e-02	1.77	20	40	1808	1.12e-02	1.05e-02	2.86e-03	1.18
3	33	40	1409	1.30e-02	9.92e-03	1.04e-02	1.56	24	160	7796	2.80e-03	2.79e-03	2.05e-03	1.72
4	42	88	3842	7.38e-03	5.15e-03	1.02e-02	2.07	28	316	14340	1.58e-03	7.02e-04	1.44e-03	1.35
5	54	88	4854	6.64e-03	5.32e-03	6.55e-03	1.78	33	316	16990	1.52e-03	7.59e-04	1.07e-03	1.19
6	70	160	8788	4.16e-03	3.12e-03	5.54e-03	2.08	46	544	39612	8.79e-04	4.08e-04	5.04e-04	1.03
7	91	160	11395	4.03e-03	3.06e-03	4.07e-03	1.76	55	820	74310	5.15e-04	2.02e-04	3.77e-04	1.12
8	105	160	16357	3.16e-03	2.15e-03	3.78e-03	1.87	66	820	89752	4.87e-04	2.03e-04	2.56e-04	0.94

Table 5.2: Adaptive refinement including effectivity indices with goal quantity J_Q , $\varepsilon = 1$, $\delta_0 = 0$, and $\omega = 1.5$ for Example 1, using a **higher-order finite elements** strategy for the temporal weights.

Example 2: Moving Hump with Circular Layer The second example is a benchmark for convection-dominated problems that goes back to [15]. The (analytical) solution is characterized by a hump changing its height in the course of the time, given by (cf. [8, Ex. 4.3])

$$u(\mathbf{x}, t) := \frac{16}{\pi} \sin(\pi t) x_1 (1 - x_1) x_2 (1 - x_2) \cdot \left(\frac{1}{2} + \arctan \left[2\varepsilon^{-\frac{1}{2}} (r_0^2 - (x_1 - x_1^0)^2 - (x_2 - x_2^0)^2) \right] \right) \quad (5.2)$$

The problem is defined on $\Omega \times I := (0, 1)^2 \times (0, 0.5]$ with the scalars $r_0 = 0.25$ and $x_1^0 = x_2^0 = 0.5$. We choose $\mathbf{b} = (2, 3)^\top$ and $\alpha = 1$. The goal quantity is chosen to control the L^2 -

error $e_N^- = u(\mathbf{x}, T) - u_{\tau h}(T^-)$, at the final time point T , given by $J_T(u) = (u(\mathbf{x}, T), e_N^-) / \|e_N^-\|$. In Fig. 5.1, we compare both approximation approaches regarding the development of the

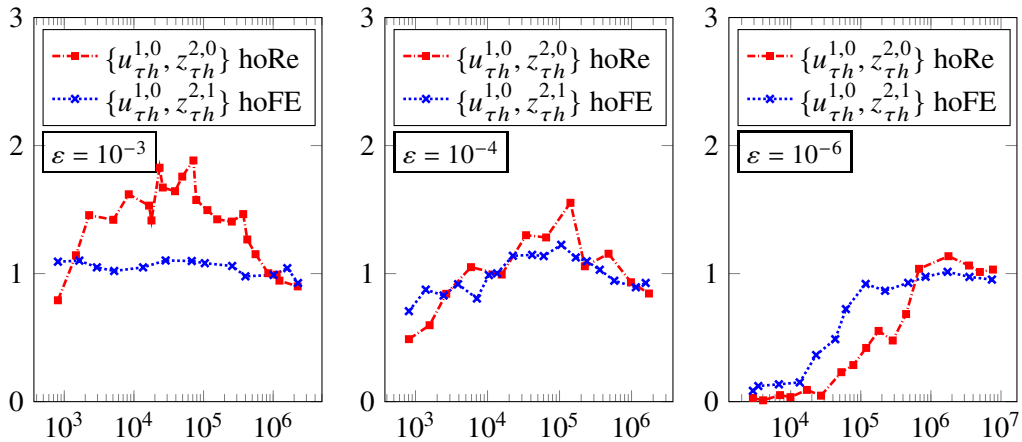


Figure 5.1: Comparison of effectivity indices \mathcal{I}_{eff} (over total space-time DoFs) regarding both approximation approaches for varying diffusion coefficients ε , using $\delta_0 = 1$, $\omega = 2$ and J_T for Example 2.

respective effectivity indices for a sequence of decreasing diffusion coefficients. Overall, the desired value of one is reached in the course of the refinement process for both approaches in all considered cases of ε , but there are slight differences with regard to accuracy, efficiency and stability reasons. For $\varepsilon = 10^{-3}, 10^{-4}$, we observe a slight overestimation of the exact error by using the hoRe approach. In contrast, the hoFE approach seems to be more stable. The more challenging case of $\varepsilon = 10^{-6}$ shows a slightly different behavior. Here, both approaches show up with small values for the effectivity index at the beginning. It takes some refinement processes until this value increases. Again, the hoFE approach shows slightly better results with regard to accuracy and efficiency evident by an faster achievement of the desired value of one. This behavior is in good agreement to the results obtained for the steady-state case, even though the differences between the both approaches is not that significant here, cf. Example 1 in [6] and [8, Ch. 3].

6 Conclusion

In this work, we compared two different approaches for approximating the temporal weights occurring within the error estimators based on the DWR method. We studied accuracy, efficiency and stability reasons by means of a convection-dominated model problem. Robustness of the underlying space-time adaptive algorithm was shown and effectivity indices close to one were obtained for both approximation techniques. Even though the higher-order finite elements approach shows slightly better results with regard to accuracy and stability (cf. Fig. 5.1), the differences to the higher-order reconstruction approach in all was not that significant as for the steady-state case (cf. [6, 8]), even less if we take into account the higher computational costs for solving the dual problem.

Acknowledgement

We acknowledge U. Köcher for his support in the design and implementation of the underlying software `dwr-condiffrea`; cf. the software project `DTM++.Project/dwr` [16] that is based on the open source finite element library `deal.II` [17].

Appendix

The SUPG stabilization terms for the stabilized primal problem (2.4) are defined as

$$\begin{aligned}
S_A(u_{\tau h})(\varphi_{\tau h}) &:= \sum_{n=1}^N \int_{I_n} \sum_{K \in \mathcal{T}_h} \delta_K(r(u_{\tau h}), \mathbf{b} \cdot \nabla \varphi_{\tau h})_K \, dt \\
&+ \sum_{n=2}^N \sum_{K \in \mathcal{T}_h} \delta_K([u_{\tau h}]_{n-1}, \mathbf{b} \cdot \nabla \varphi_{\tau h, n-1}^+)_K + \sum_{K \in \mathcal{T}_h} \delta_K(u_{\tau h, 0}^+ - u_0, \mathbf{b} \cdot \nabla \varphi_{\tau h, 0}^+)_K, \\
r(u_{\tau h}) &:= \partial_t u_{\tau h} + \mathbf{b} \cdot \nabla u_{\tau h} - \nabla(\varepsilon \nabla u_{\tau h}) + \alpha u_{\tau h} - f.
\end{aligned}$$

Remark 6.1 For time-dependent convection-diffusion problems an optimal error estimate for $\delta_K = O(h_K)$ is derived in [18].

The Lagrangian functionals $\mathcal{L} : V \times V \rightarrow \mathbb{R}$, $\mathcal{L}_\tau : V_\tau^r \times V_\tau^r \rightarrow \mathbb{R}$, and $\mathcal{L}_{\tau h} : V_{\tau h}^{r,p} \times V_{\tau h}^{r,p} \rightarrow \mathbb{R}$ are defined by

$$\begin{aligned}
\mathcal{L}(u, z) &:= J(u) + F(z) - A(u)(z), \\
\mathcal{L}_\tau(u_\tau, z_\tau) &:= J(u_\tau) + F(z_\tau) - A_\tau(u_\tau)(z_\tau), \\
\mathcal{L}_{\tau h}(u_{\tau h}, z_{\tau h}) &:= J(u_{\tau h}) + F(z_{\tau h}) - A_S(u_{\tau h})(z_{\tau h})
\end{aligned} \tag{6.1}$$

Here, the Lagrange multipliers z , z_τ , and $z_{\tau h}$ are called dual variables in contrast to the primal variables u , u_τ , and $u_{\tau h}$; cf. [13, 2]. Considering the directional derivatives of the Lagrangian functionals, also known as Gâteaux derivatives, with respect to their first argument, i.e. $\mathcal{L}'_u(u, z)(\varphi) := \lim_{t \neq 0, t \rightarrow 0} t^{-1} \{ \mathcal{L}(u + t\varphi, z) - \mathcal{L}(u, z) \}$, $\varphi \in V$, leads to the dual problems: Find the continuous dual solution $z \in V$, the semi-discrete dual solution $z_\tau \in V_\tau^r$ and the fully discrete dual solution $z_{\tau h} \in V_{\tau h}^{r,p}$, respectively, such that

$$\begin{aligned}
A'(u)(\varphi, z) &= J'(u)(\varphi) \quad \forall \varphi \in V, \\
A'_\tau(u_\tau)(\varphi_\tau, z_\tau) &= J'(u_\tau)(\varphi_\tau) \quad \forall \varphi_\tau \in V_\tau^r, \\
A'_S(u_{\tau h})(\varphi_{\tau h}, z_{\tau h}) &= J'(u_{\tau h})(\varphi_{\tau h}) \quad \forall \varphi_{\tau h} \in V_{\tau h}^{r,p},
\end{aligned} \tag{6.2}$$

where we refer to our work [8, Ch. 4.2.1] for a detailed description of the adjoint bilinear forms A' , A'_τ , A'_S as well as the dual right hand side term J' . Finally, the primal residual based on the semi-discrete scheme is defined by means of the Gâteaux derivatives of the Lagrangian functionals in the following way:

$$\rho_\tau(u)(\varphi) := \mathcal{L}'_{\tau, z}(u, z)(\varphi) = G_\tau(\varphi) - A_\tau(u)(\varphi),$$

References

- [1] Becker, R., Rannacher, R.: Weighted a posteriori error control in FE methods. In: Bock, H.G., Kanschat, G., Rannacher, R., Brezzi, F., Glowinski, R. (eds.) ENUMATH 97. Proceedings of the 2nd European Conference on Numerical Mathematics and Advanced Applications, pp. 621-637. World Scientific, Singapore (1998)
- [2] Becker, R., Rannacher, R.: An optimal control approach to a posteriori error estimation in finite element methods. In: Iserles, A. (ed.) Acta Numer., Vol. 10, pp. 1-102. Cambridge University Press (2001) doi:10.1017/S0962492901000010
- [3] Ahuja, K., Endtmayer, B., Steinbach, M.C., Wick, T.: Multigoal-oriented error estimation and mesh adaptivity for fluid-structure interaction. J. Comput. Appl. Math. **412**:114315, (2022) doi:10.1016/j.cam.2022.114315

- [4] Braak, M., Richter, T.: Solutions of 3D Navier-Stokes benchmark problems with adaptive finite elements. *Comput. Fluids* **35**(4), 372–392 (2006) doi:10.1016/j.compfluid.2005.02.001
- [5] Meidner, D., Vexler, B.: Adaptive space-time finite element methods for parabolic optimization problems. *SIAM J. Control Optim.* **46**(1), 116–162 (2007) doi:10.1137/060648994
- [6] Bruchhäuser, M.P., Schwegler, K., Bause, M.: Numerical study of goal-oriented error control for stabilized finite element methods. In: Apel, T. et al. (eds.) *Advanced Finite Element Methods with Applications. FEM 2017. Lecture Notes in Comput. Sci. Eng.*, vol. 128, pp.85-106. Springer, Cham (2019). doi:10.1007/978-3-030-14244-5_5
- [7] Ern, A., Guermond, J.-L.: *Finite elements III: First-order and time-dependent pdes.* vol. 74, *Texts in Applied Mathematics*, Springer, Cham (2021)
- [8] Bruchhäuser, M.P.: *Goal-Oriented Space-Time Adaptivity for a Multirate Approach to Coupled Flow and Transport*, Dissertation, Helmut-Schmidt-University, University of the German Federal Armed Forces Hamburg (2022) doi:10.24405/14380
- [9] Bangerth, W., Rannacher, R.: *Adaptive finite element methods for differential equations.* Birkhäuser, Basel (2003) doi:10.1007/978-3-0348-7605-6
- [10] Hughes, T.J.R., Brooks, A.N.: A multidimensional upwind scheme with no crosswind diffusion. In: Hughes, T.J.R. (ed.) *Finite Element Methods for Convection Dominated Flows*, AMD, vol. 34, Amer. Soc. Mech. Engrs. (ASME), 19–35 (1979)
- [11] Brooks, A.N., Hughes, T.J.R.: Streamline upwind/Petrov-Galerkin formulations for convection dominated flows with particular emphasis on the incompressible Navier-Stokes equations. *Comput. Methods Appl. Mech. Eng.* **32**(1-3), 199–259 (1982)
- [12] Richter, T.: *Fluid-structure interactions: Models, analysis and finite elements*, *Lect. Notes Comput. Sci. Eng.* **118**, Springer, Berlin (2017)
- [13] Besier, M., Rannacher, R.: Goal-oriented space-time adaptivity in the finite element Galerkin method for the computation of nonstationary incompressible flow. *Int. J. Num. Methods Fluids* **70**(9), 1139–1166 (2012) doi:10.1002/fld.2735
- [14] Bruchhäuser, M.P., Köcher, U., Bause, M.: On the implementation of an adaptive multirate framework for coupled transport and flow. *J. Sci. Comput.* **93**, 59 (2022) doi:10.1007/s10915-022-02026-z
- [15] John, V., Schmeyer, E.: Finite element methods for time-dependent convection-diffusion-reaction equations with small diffusion. *Comput. Methods Appl. Mech. Eng.* **198**(3-4), 475–494 (2008) doi:10.1016/j.cma.2008.08.016
- [16] Köcher, U., Bruchhäuser, M.P., Bause, M.: Efficient and scalable data structures and algorithms for goal-oriented adaptivity of space-time FEM codes, *Software X*, 10:100239 (2019) doi:10.1016/j.softx.2019.100239
- [17] Arndt, D., Bangerth, W., Blais, B., Fehling, M., Gassmüller, R., Heister, T., Heltai, L., Köcher, U., Kronbichler, M., Maier, M., Munch, P., Pelteret, J.-P., Proell, S., Simon, K., Turcksin, B., Wells, D., Zhang, J.: The deal.II Library, Version 9.3. *J. Numer. Math.* **29**(3), 171–186 (2021)

- [18] John, V., Novo, J.: Error analysis of the SUPG finite element discretization of evolutionary convection-diffusion-reaction equations. *SIAM J. Numer. Anal.* **49**(3), 1149–1176 (2011)